REVIEW

Unraveling Vibrational Wavepacket Dynamics using Femtosecond Ion Yield Spectroscopy and Photoelectron Imaging†

Bing Zhang*

State Key Laboratory of Magnetic Resonance and Atomic and Molecular Physics, Wuhan Institute of Physics and Mathematics, Chinese Academy of Sciences, Wuhan 430071, China

(Dated: Received on November 15, 2018; Accepted on December 6, 2018)

Time-resolved photoionization is a powerful experimental approach to unravel the excited state dynamics in isolated polyatomic molecules. Depending on species of the collected signals, different methods can be performed: time-resolved ion yield spectroscopy (TR-IYS) and time-resolved photoelectron imaging (TR-PEI). In this review, the essential concepts linking photoionization measurement with electronic structure are presented, together with several important breakthroughs in experimentally distinguishing the oscillating wavepacket motion between different geometries. We illustrate how femtosecond TR-IYS and TR-PEI are employed to visualize the evolution of a coherent vibrational wavepacket on the excited state surface.

Key words: Vibrational wavepacket, Time-resolved ion yield, Photoelectron imaging, Excited state dynamics

I. INTRODUCTION

There is considerable interest in the excited state dynamics of molecules following irradiation with ultraviolet (UV) light due to its significance in chemistry and biology; representative examples include stabilization of DNA against UV-radiation [1], vision and photosynthesis [2]. An understanding of excited-state photochemistry is not only of fundamental importance to gain insight into the dynamics of unimolecular reactions, but also serves as a stepping stone for establishing the structure-dynamics-function relationship in large chemical and biological systems. It is recognized that experiments on isolated molecules in the gas-phase, free from interactions with a solvent or protein microenvironment, allow the intrinsic properties of a molecule to be studied in great detail. Such a bottom-up approach initially investigates the building blocks of larger complexes without the natural environment and then systematically probes effects of the increased complexity on the dynamics, providing an important starting point for studying complex systems [3].

Based on the seminal studies of Zewail and co-workers [4, 5], an explosion, in the application of ultrafast lasers to track chemical reactions with femtosecond resolution, has been witnessed in the past few years [6, 7]. This methodology has been applied to chemical reactions ranging in complexity from bond breaking in diatomic molecules to intricate dynamics in large biological and inorganic systems, and has led to significant breakthroughs in the studies of fundamental chemical processes. Most of the experiments with femtosecond resolution involve a pump-probe framework in which an ultrafast pump pulse is used to initiate a reaction or, more generally, creates a nonstationary state, the evolution of which is observed by interaction with a time-delayed probe pulse. A variety of ultrafast techniques are hence emerging to follow the molecular dynamics, such as resonant multiphoton ionization and laser-induced fluorescence in the gas phase, transient absorption spectroscopy and nonlinear optical spectroscopy in the condensed phase, and time-resolved X-ray or electron diffraction with ultrafast X-ray or electron pulses in both condensed and gas phases [8–11]. Here, we focus upon gas-phase time-resolved ion yield spectroscopy (TR-IYS) and time-resolved photoelectron imaging (TR-PEI) of neutral polyatomic molecules. In general, each of the two methods is very important and complements the other. For example, ion-yield measurements are very useful for monitoring the generation of products and identifying any transient species [12], whereas TR-PEI provides an additional level about the energy information of these species as a function of time.

Using femtosecond TR-IYS and TR-PEI, one can follow a host of electronic and vibrational dynamics of isolated molecules, such as quantum control [13, 14], isomerization [15, 16], photodissociation [17, 18], proton transfer [19, 20], hydrogen tunneling [21, 22], internal conversion (IC) [23, 24], intersystem crossing (ISC)

†Dedicated to Professor Kopin Liu on the occasion of his 70th birthday.

*Author to whom correspondence should be addressed. E-mail: bzhang@wipm.ac.cn

[25, 26], intramolecular vibrational energy redistribution (IVR) [27, 28], and coherent wavepacket motion [29, 30]. A number of recent reviews have concentrated on the use of time-resolved photoelectron spectroscopy to investigate the electronic relaxation dynamics of photoexcited molecules [3, 31–38]. The focus of the present review is on the application of femtosecond TR-IYS and TR-PEI as a tool for probing the coherent wavepacket motion on the excited state surface. Based on the uncertainty principle [39], the femtosecond laser pulses with ultrashort pulse width should possess a broad optical spectrum. This indicates, therefore, that photoexcitation with a femtosecond pulse will encompass several adjacent vibrational states simultaneously within a given molecular excited state, and thus prepare a coherent superposition of the vibrational eigenstates, resulting in a time-evolving vibrational wavepacket [40]. A time-dependent wavepacket composed of n vibrational wavefunctions (Ψ_n) can be expressed mathematically as follows [34]:

$$|\Psi(t)\rangle = \sum_n A_n \mathrm{e}^{-iE_n t/\hbar} |n\rangle \tag{1}$$

where E_n is the energy of the n wavefunction, and A_n is a scaling factor. Following initial photoexcitation, the individual wavefunctions will interfere constructively, resulting in a localized vibrational envelope with high amplitude in the vertical Franck-Condon (FC) region and near zero amplitude on other areas of the potential energy surface (PES). The time-dependency of the above equation causes the position at which the constructive interference occurs to change as a function of time, resulting in the wavepacket moving as a coherent entity and oscillating on the PES. Hence, the coherent nuclear motion initiated by evolution of the vibrational wavepacket is manifested as the quantum beat-modulated decay. The beat arises from the quantum interferences among those eigenstates comprising the vibrational wavepacket [13]. If the probing transition is sensitive to the position of constructive interference, *i.e.*, evolution of the vibrational wavepacket, the measured signals will unravel the vibrational wavepacket dynamics in real time. With this overview in mind, the rest of this review will illustrate how femtosecond TR-IYS and TR-PEI are employed to visualize the evolution of a coherent vibrational wavepacket in photoexcited molecules.

II. EXPERIMENT AND CALCULATION

As the chosen examples in this review are mainly based on a combination of experimental methods and theoretical calculations, our discussion begins with a brief overview of the methodologies used to track the vibrational wavepacket dynamics of isolated molecules. For excellent reviews containing further details, the reader is referred to Refs.[3, 31–33, 36–38].

A. Time-resolved ion yield spectroscopy

The simplest measurement employed to unravel the excited state dynamics in real time is TR-IYS, which can be concisely summarized as a powerful combination of femtosecond pump-probe spectroscopy with mass-resolved ion detection. A first femtosecond pump pulse is used to promote an isolated molecule to the excited electronic states, of which the evolution is projected onto the cationic state by a second femtosecond probe pulse. In general, a chosen target molecule is seeded in helium gas at a pressure of more than 1 bar and expands into the vacuum through a pulsed nozzle to generate the supersonic molecular beam. The base pressure of the vacuum is maintained below 2×10^{-6} Torr. After collimation by using a skimmer, the pulsed molecular beam is introduced into the ionization chamber and interacted with femtosecond laser pulses in the center of a time-of-flight (TOF) arrangement [41]. The resulting ions are accelerated into a field-free region by a set of electrostatic immersion lenses and then detected by a position-sensitive detector consisting of a dual-microchannel plate and a phosphor screen. The TOF spectra are recorded by monitoring the current output directly from the phosphor screen using an oscilloscope. The measurements of parent ion and fragment ions directly identify some transient species under interrogation and provide much information on dissociation pathways in photoexcited molecules [4]. Then the temporal profiles of these ions are recorded as a function of pump-probe time delay, Δt. By fitting the data with a sum of exponential functions convoluted with a Gaussian cross-correlation function [37], we can extract the lifetime of the involved dynamical processes.

B. Time-resolved photoelectron imaging

Although TR-IYS can offer rich insight into the kinetics of processes, its integral nature limits the ability to distinguish the individual behaviors of specific states. With the advent of charged-particle imaging [42] and specifically photoelectron imaging (PEI) [43], the investigation of excited state dynamics has made a great advancement. The combination of pump-probe spectroscopy with PEI, *i.e.*, TR-PEI, enables one to extract both kinetic energy information and angular distributions [36, 44], which are crucial to identify the origin of the generated electrons. In a TR-PEI experiment, an ultrashort pump laser pulse promotes a molecule to the excited electronic states and after a predetermined time delay a second ultrashort probe laser "interrogates" the molecular system. The ensuing electron avalanche strikes a phosphor screen and is then imaged by a charge-coupled-device camera. Various image reconstruction techniques [45–47] can be used to recover the full three-dimensional distribution from the measured two-dimensional image. Considering that ioniza-

DOI:10.1063/1674-0068/cjcp1811252

tion is always an allowed process, TR-PEI is often described as a universal method to track the electronic dynamics [38]. In principle, the initially excited state and the intermediate products can be probed and distinguished by their characteristic photoelectron kinetic energy (PKE) and photoelectron angular distribution (PAD). More importantly, changes in the kinetic energy and angular distribution will be detected with great sensitivity and act as an indicator of the evolving molecular structure at the time that electrons are ejected [48, 49]. In this way, nuclear motion of the photoexcited molecules is recorded in the molecular frame and in real time.

C. The computational methodology

In order to interpret the experimental results and gain further insight into the intrinsic properties of the target molecule, quantum chemistry calculations are performed to determine the electronic energies and nuclear geometries of key features on the potential energy landscape as well as ionization energies. In this review, the special emphasis is laid upon optimization of the minimum-energy structures of the electronic ground state (S_0), the first excited singlet electronic state (S_1), and the cationic ground state (D_0). In brief, the calculations are performed using the Gaussian 09 computational package, and the geometries are optimized with density functional theory (DFT) for the S_0 and D_0 states but time-dependent density functional theory (TD-DFT) for the S_1 state at the theory levels of B3LYP/TD-M052X/CAM-B3LYP.

III. CASE STUDIES

There are a great number of examples where time-resolved photoionization experiment is combined with computational methods to unravel the electronic relaxation dynamics in photoexcited molecules, some of which have been discussed in other reviews. In this review, we choose some typical cases to illustrate its application in the detailed vibrational wavepacket dynamics on the excited state surface.

A. Catechol

We begin our illustration on the wavepacket dynamics by presenting experimental work carried out on catechol, one of the chromophore building blocks of several biologically relevant species [50, 51]. According to the "bottom-up" study [3], the photoinduced dynamics in small molecules provides an important starting point for studying nuclear motions of complex systems. For instance, excited state dynamics of the catechol chromophore has been the subject of many spectroscopic investigations [52–54]. It was revealed that, following photoexcitation to the origin of the S_1 state, catechol underwent a tunneling process via the conical intersection between the bound $S_1(^1\pi\pi^*)$ and dissociative $S_2(^1\pi\sigma^*)$ potential-energy surfaces in the O−H coordinate. Importantly, the O−H fission mediated by this tunneling mechanism occurred on a picosecond time scale [52]. In order to visualize the nuclear motions that happened before, and during, the tunneling process, Stavros *et al.* utilized the nonplanar→planar structural change upon ionization as an effective FC detection window [55]. The minimum-energy geometries of the ground, excited, and ionic states were optimized using the CAM-B3LYP functional with an aug-cc-pVDZ basis set. As shown in FIG. 1(a), although the minimum geometries of the S_0 and D_0 states were both planar, the equilibrium geometry of the S_1 state ($S_{1,min}$) was nonplanar, where the free O−H bond lies at an angle of ∼14° out of the phenyl ring plane.

Upon UV irradiation at 280.5 nm, a coherent superposition of low-lying FC-active torsional motions was excited in S_1, leading to a localized vibrational wavepacket. The typical time-resolved ion yield (TR-IY) transient (FIG. 1(b)) recorded following ionization at 328 nm exhibited a superimposed oscillation, which was attributed to variation in the ionization probability as the vibrational wavepacket evolved on the S_1 surface. These oscillations, known as a quantum beat, arose from coupling between a few vibrational states. The fast Fourier transform (FFT) of the transient yielded three frequency components with associated energies centered at 113, 141, and 250 cm^{-1}, corresponding to periodicities of 295, 237, and 133 fs. The observed frequencies aligned well with the wave number separations in the vibrational progression of the low-lying O−H torsional mode (τ_2). Stavros *et al.* proposed that the selection of probe wavelength was the critical factor of the final observable. The total energy (E_{tot}) of the 280.5 nm pump and 328 nm probe pulses was slightly above the adiabatic ionization potential (IP_{ad}), which in catechol laid at 8.17 eV [56].

Considering that there were obvious differences in geometry between the S_1 and D_0 states, the ionization cross section was variable along the torsional coordinate. The prepared vibrational wavepacket oscillated along the O−H torsional coordinate; however, the probe photon energy was just sufficient to ionize the molecules at or around planar geometries. Note that it was the effective FC window created by the geometry change upon photoionization that enabled one to probe the coherent nuclear motion and observe a quantum beat using TR-IYS. In addition, the contribution of individual components in the coherent superposition could be manipulated by tuning the pump-pulse wavelength. Following excitation at 281.5 nm and probing with 326.6 nm, the measured transient was superimposed by a single quantum beat with the frequency at 116 cm^{-1} which corresponded to the wavenumber separation between the S_1 origin and one quantum vibrational progression of τ_2. This study demonstrated the

DOI:10.1063/1674-0068/cjcp1811252

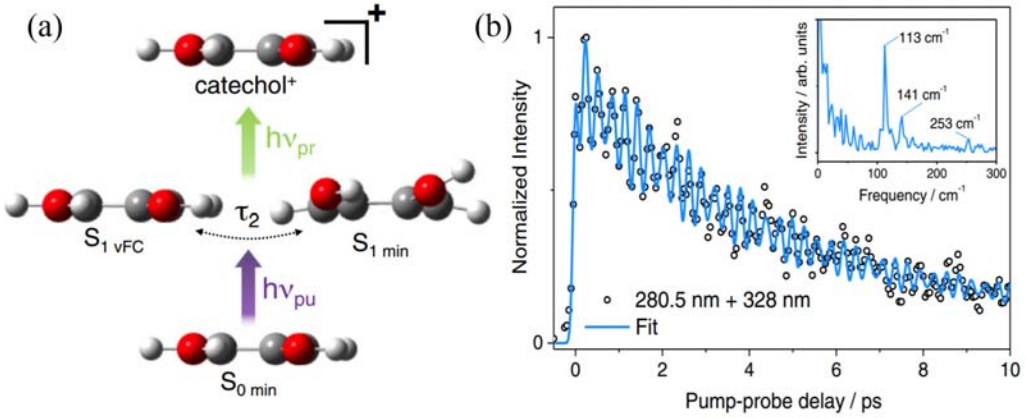

FIG. 1 (a) Schematic representation of nuclear geometries during the pump-probe processes in catechol calculated using the CAM-B3LYP functional with an aug-cc-pVDZ basis set. (b) TR-IY transient collected from catechol following excitation at 280.5 nm and subsequent ionization with 328 nm. Inset: The FFT of the transient. Reprinted with permission from Ref.[55]. Copyright 2015 American Physical Society (https://creativecommons.org/licenses/by/3.0/).

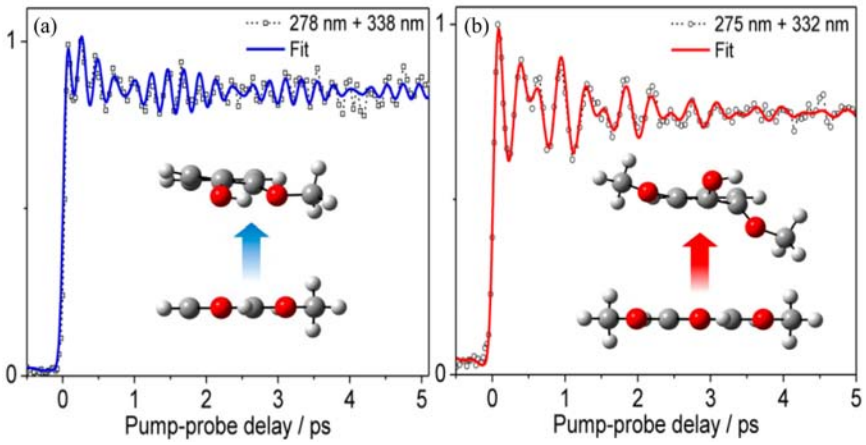

FIG. 2 The time-resolved ion yield transients collected from (a) guaiacol and (b) syringol at the selected pump and probe wavelengths. The insets show the calculated geometries in the S_0 and S_1 states using TDM05-2X/6-311++G(d,p). Reprinted with permission from Ref.[57]. Copyright 2014 American Chemical Society.

sensitivity of TR-IYS to probe the nuclear motions of a molecule as the wavepacket evolved on the excited state surface and emphasized the critical roles of the geometry changes between electronic states and the choice of probe wavelengths.

B. Guaiacol and syringol

Lignin is the second abundant naturally occurring biopolymer only to cellulose in plants. However, due to the complexity of the system itself, our knowledge of the precise complete structure-function relationships is still lacking. Stavros *et al.* proposed a bottom-up approach as a first step toward understanding UV-induced photodegradation pathways within lignin in great detail [57]. Note that guaiacol and syringol are important structural units of lignin. The detailed description of relative photostabilities in small building blocks such as guaiacol and syringol can be therefore used as stepping stones for investigating the structure-dynamics-function picture within bigger biological systems such as lignin. Following photoexcitation at 278 nm, guaiacol was excited to its S_1 origin and the ensuing dynamics was probed via single photon ionization at 338 nm. As shown in FIG. 2(a), an exponentially damped oscillation was superimposed on the guaiacol$^+$ transient. Quantum calculations performed at the TD-M052X level with a 6-311++G(d,p) basis set indicated that the guaiacol molecule underwent the planar→nonplanar ($S_{0,min}$→$S_{1,min}$) geometry change upon photoexcitation (inset of FIG. 2(a)). The FFT of the transient revealed that the beat contained two dominant frequencies with associated energies of 143 and 163 cm^{-1} (corresponding to periodicities of 233 and 205 fs, respec-

DOI:10.1063/1674-0068/cjcp1811252

tively), which agreed reasonably well with the known band separations in an even quanta vibrational progression of the out-of-plane methoxy (OMe) "flapping" mode (φ) [58–60]. Therefore, the pronounced beating in φ could be understood as follows. After excitation from the planar $S_{0,min}$ geometry, a coherent superposition of out-of-plane OMe flapping motions was prepared in the S_1 state, resulting in a time-evolving vibrational wavepacket. By virtue of a dramatic nonplanar→planar ($S_{1,min}$→guaiacol$^+$) geometry change upon photoionization, the evolution of the vibrational wavepacket was accompanied by the variable ionization cross section along φ, resulting in the characteristic beat seen in FIG. 2(a). Once again, this was directly in line with previous vibrational wavepacket studies in catechol [55]. The adequate FC detection window required by the quantum beat detection was also afforded by the structural distortion between the S_1 (nonplanar) and D_0 (planar) geometries and very sensitive to the probe wavelength.

FIG. 2(b) showed the time-resolved syringol$^+$ signal formed following excitation at 275 nm and subsequent ionization using 332 nm. With guaiacol, there was a clear beat in the transient. The FFT of the data exhibited two major frequency components at 78 and 112 cm^{-1}, corresponding to periodicities of 428 and 298 fs, respectively. According to the known resonance enhanced multi-photon ionization (REMPI) spectrum of syringol [58], the observed frequencies most likely arose from the coherent excitation of the S_1 origin and combination modes involving the OMe torsion (τ_{OMe}) and φ modes. Observation of these quantum beats was also based on the presence of an FC detection window. The TD-DFT calculations on syringol predicted that at the nonplanar $S_{1,min}$ geometry, the H-bonded OMe group distorted ∼50° out-of-plane in one direction, while the OH group bent ∼25° in the other direction. However, the nonplanarity of the $S_{1,min}$ geometry was less pronounced in guaiacol. Therefore, the modulation magnitude in ionization efficiency was expected to be weakened due to the smaller displacement between the S_1 and D_0 geometries in guaiacol. In addition, the large out-of-plane distortion of its OH and OMe groups in syringol would necessarily weaken the intramolecular H bond. Considering that the photostabilities of the chromophore sites were primarily determined by the degree of H bonding preserved after the geometry rearrangement process in S_1, the order of their relative photostabilities could be roughly described as guaiacol>syringol. This study provided a first step toward understanding a more complete structure-dynamics-function picture of photodegradation in lignin.

C. CS_2

As a prototypical linear molecule, the photoinduced intramolecular dynamics of CS_2 have been the subject of many spectroscopic investigations [48, 61–67]. Using TR-PEI with a sub-20 fs 159 nm probe pulse, Suzuki *et al.* studied the wavepacket motion of CS_2 after photoexcitation to the $^1B_2$ state at 198 nm [68]. The employment of the 159 nm probe pulse enlarged considerably the observation region of the $^1B_2$ potential energy surface. The temporal profile of the total photoelectron signal was primarily a single exponential decay with some oscillatory components. The FFT of the profile revealed the major component at 400 cm^{-1}, which corresponded to unresolved symmetric (ν_1=392 cm^{-1}) and bending (ν_2=426 cm^{-1}) modes of CS_2 [62]. FIG. 3(a) showed the time-energy map of the PKE distribution. The photoelectron spectrum at Δt=0 fs exhibited the maximum intensity at around 3.8 eV, and it shifted down to 1.5 eV after about 40 fs and returned back to 3.8 eV at 80 fs. As seen in FIG. 3(c), the time-energy map of the photoelectron anisotropy parameter (β_2) also exhibited clear time and energy variations. At zero pump-probe delay time, β_2 had its lowest value of −0.1 at 3.8 eV and its lowest value of 0.4 at 1 eV. The variation of anisotropy arose from excitation amplitudes of partial waves that changed with the time-dependent wavefunction in the excited states [68]. Therefore, time dependence of β_2 at a given PKE was attributed to variation of the excited states electronic character along the ν_1 and ν_2 coordinates. The power spectrum of the anisotropy (inset of FIG. 3(c)) had two distinct frequencies: 40 and 400 cm^{-1}. The low frequency corresponded to the beat between ν_1 and ν_2 while the high frequency was assigned to the unresolved ν_1 and ν_2 vibrations.

From the above discussion, it was clear that the 198 nm pump laser pulse promoted the CS_2 molecule to the $^1B_2$ state with vibrational excitation of the ν_1 and ν_2 modes. Since the D_0 state possessed almost the same equilibrium geometry as the S_0 state [69], photoionization from the linear geometry in the FC region occurred to low vibrational states in D_0, producing photoelectrons with kinetic energy of 4.0 eV. After 40 fs, which corresponded to a half period of ν_1 and ν_2 vibrations, photoionization was induced from the bent and stretched geometry. Since the $^1B_2$ state had a bent (153°) equilibrium geometry with an elongated C−S bond length (1.66 Å) compared to that of linear D_0 with a C−S bond length of 1.555 Å [69], photoionization from this largely distorted geometry had good FC overlap with vibrationally excited states in D_0, generating photoelectrons with kinetic energy of 1.5 eV. The initial change in the time-resolved photoelectron spectra corresponded to the motion from the linear geometry in the FC region to the bent and stretched equilibrium geometry. The photoelectron intensity power spectrum exhibited two major components at 391 and 426 cm^{-1} due to the ν_1 and ν_2 vibrations. Therefore, the observed photoelectron oscillations were the direct manifestation of the wavepacket dynamics of the ν_1 and ν_2 vibrations.

DOI:10.1063/1674-0068/cjcp1811252

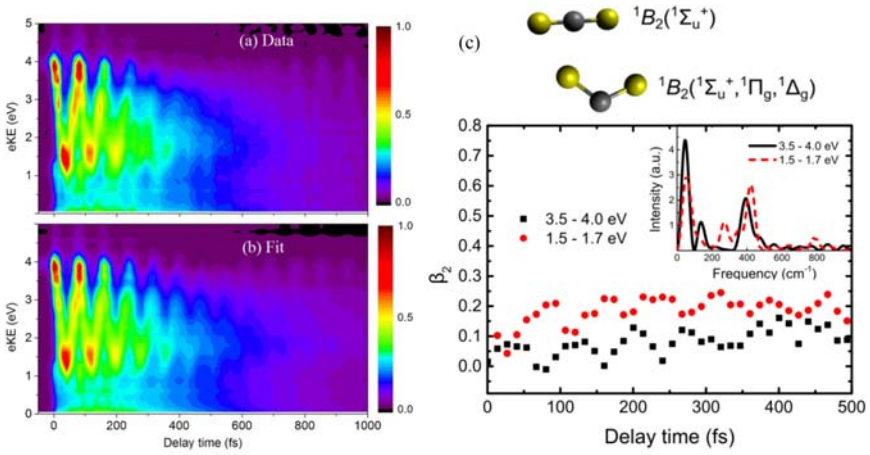

FIG. 3 The time-energy map of the PKE distribution: (a) experimental data and (b) fit. (c) Time dependences of the β_2 coefficients integrated over the 3.5−4.0 eV and 1.5−1.7 eV PKE ranges. The inset shows the corresponding frequency spectra obtained from the FFT. Reprinted with permission from Ref.[68]. Copyright 2015 American Institute of Physics.

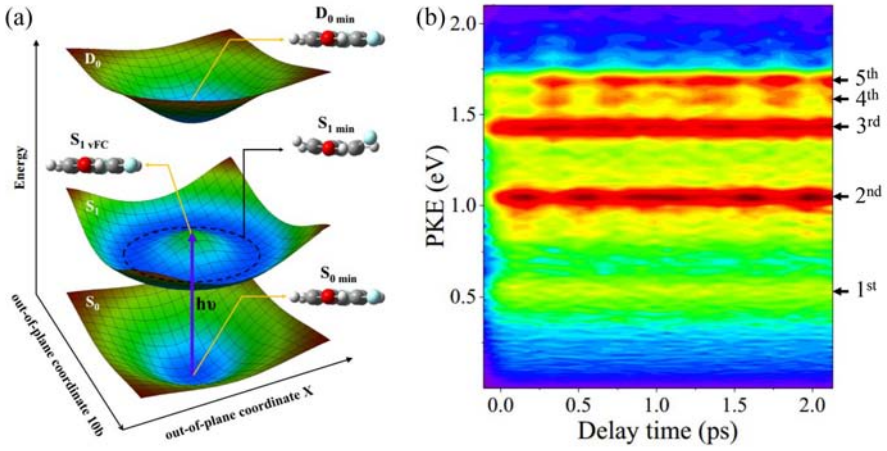

FIG. 4 (a) Schematic diagram of the ground, excited, and ionic states potential surfaces along the out-of-plane bending coordinates X and 10b, together with the calculated structures using CAM-B3LYP/aug-cc-pVDZ. (b) Photoelectron time-energy map of 2,4-DFP pumped with 279.9 nm and probed with 400 nm. Reprinted with permission from Ref.[70]. Copyright 2017 American Physical Society.

D. 2,4-Difluorophenol

In the following sections, we will choose to illustrate the application of TR-IYS and TR-PEI on investigating wavepacket dynamics using examples from our own groups. FIG. 4(a) showed the minimum-energy structures of the S_0, S_1, and D_0 states in 2,4-difluorophenol (2,4-DFP) calculated at the theory level of CAM-B3LYP with an aug-cc-pVDZ basis set [70]. The equilibrium geometries of the S_0 and D_0 states were both planar, but the minimum-energy geometry of S_1 was nonplanar in which the free F particle rotated over 31° out of the aromatic plane. Therefore, the potential energy surfaces possessed a pronounced potential well in the S_0 and D_0 states but double potential wells in the S_1 state along the out-of-plane vibrational bending coordinate X or 10b [71, 72]. After preparing a coherent vibrational wavepacket by the simultaneous excitation of the out-of-plane bending modes in 2,4-DFP, we firstly employed TR-IYS to probe the coherent vibrational motion accompanied with structural changes along the reaction coordinate. By virtue of the geometry changes upon photoionization, evolution of the coherent wavepacket was efficiently detected with appropriate probe wavelengths, presenting as the pronounced quantum beats superimposed on the parent-ion transients. The beats with modulation frequencies of 70 and 89 cm^{-1} were due to the quantum-interference effects created by coherent excitation of the S_1 origin, the out-of-plane vibrations X and 10b [73]. We also stressed that the superposition state composed of different vibrational bands could be selectively prepared by tuning

DOI:10.1063/1674-0068/cjcp1811252

the pump pulse wavelength. In addition, following ionization with 243 nm, such that the combined pump and probe energies far exceeded the IP_{ad} of 8.68 eV [73], the beat in the TR-IY signals for 2,4-DFP^+ disappeared, confirming the sensitivity of the detection window to the probe wavelength.

The origins of these beats were similar to the cases in catechol [55], guaiacol and syringol [57]. If the total energy was slightly above IP_{ad}, the molecules around the planar geometry were ionized exclusively. With higher probe photon energy, however, the molecules whether at planar or nonplanar geometries were both ionized and the ion-yield measurements were unable to extract the individual contributions of different geometries. However, TR-PEI provided the possibility of directly visualizing the coherent nuclear motion between different geometries due to the sensitivity of the PKE distribution to the nuclear configuration. FIG. 4(b) showed the time-energy map of the photoelectron intensities with a 279.9-nm pump and a 400-nm probe. Five sharp peaks centered at 0.54, 1.05, 1.43, 1.58, and 1.68 eV were assigned as the first to fifth peaks, respectively. Obviously, the first and second peaks exhibited the clear beats with similar periodicities but a phase shift of π rad with respect to the other three peaks. The Rydberg states involved in the ionization processes could be identified by the calculated quantum defects. Furthermore, based on analysis of the spectral features during the first 240 fs, we concluded that the first and second peaks were attributed to the accidental resonances with the 3s and 3p Rydberg states of the nonplanar geometry, and the other three rings were produced by the resonances with the 3d Rydberg states of the planar geometry. That was to say, the time-dependent spectrum in FIG. 4(b) reflected directly the vibrational wavepacket oscillating between the planar geometry and nonplanar minimum, providing a clear physical picture of the oscillatory flow of energy induced by the coherent nuclear motion between different geometries. In the present work, we demonstrated how the time-evolving vibrational wavepacket could be tracked by TR-IYS and TR-PEI under different detection mechanisms.

E. *o*-Fluorophenol

Another example of a small aromatic molecule containing an O−H group is *o*-fluorophenol, which is one of the prototypes containing an intramolecular hydrogen-bonding and has been the subject of numerous spectroscopic studies [74–81]. Upon irradiation with the femtosecond pump pulse at 271.3 nm, we excited a coherent superposition of the S_1 origin and two quanta in the out-of-plane butterfly vibration (τ) in *o*-fluorophenol, resulting in a vibrational wavepacket [82]. Subsequently, the evolution of the vibrational wavepacket was probed by multiphoton ionization at a wavelength of 802 nm. According to the calculations performed at the M052X level of theory with the aug-cc-pVDZ basis set, although the $S_{0,min}$ and $D_{0,min}$ geometries were both planar, the $S_{1,min}$ geometry was nonplanar with rotation of the free F particle over 37° out of the aromatic plane. As seen in FIG. 5(a), the time-dependent ion signal of *o*-$fluorophenol^+$ was superimposed by a pronounced quantum beat. The FFT for the transient yielded a single frequency with an associated energy centered at 109 cm^{-1}, corresponding to a periodicity of 306 fs, which agreed well with the wavenumber separation between the S_1 origin and two quanta vibrational progression of τ [78].

Subsequent TR-PEI measurements enabled us to understand the origin of these beats. FIG. 5(b) showed the time-energy map of the photoelectron intensities. The transient behaviors of photoelectron peaks were directly related to variation of the molecular configuration at the instant of ionization. It was obvious that a superimposed coherent oscillation could be observed for all the photoelectron peaks. Furthermore, the 1st, 2nd, 3rd, and 4th peaks exhibited a similar changing trend in intensity with time, but their phase was different from that for the other peaks. On the basis of the calculated quantum defects and the spectral features during the first 153 fs, we concluded that the 1st, 2nd, 3rd, and 4th peaks were attributed to different ion vibrational states which had good FC overlap with the planar $S_{1,vFC}$ geometry, but the other peaks were assigned to photoionization from the nonplanar minimum via the resonances with the 3s and 3p Rydberg states. By the accidental resonances with intermediate Rydberg states, the ionization cross section from the nonplanar minimum was significantly enhanced. As the wavepacket oscillated along τ, variation of the molecular geometries altered the photoionization channel, resulting in the periodic changes in both the ionization efficiency and the PKE distribution. The periodic variation in the ionization probability with the geometry led to the superimposed beat in the parent-ion transient, and the change in the PKE distribution was characterized as the out-of-phase beats in the time-resolved photoelectron spectra. These beats were the direct manifestation of the vibrational wavepacket motion and the oscillatory flow of energy on the excited state surface.

F. Pyrimidine

The spectroscopic information of pyrimidine has been widely investigated for the past few decades using a variety of techniques [83–88]. Pyrimidine is not only a structural motif of three DNA/RNA bases: cytosine, thymine, and uracil [89], but also found in other natural derivatives and synthetic compounds. By using a combination of TR-IYS and TR-PEI measurements, we demonstrated the application of FC filters to visualize the vibrational wavepacket dynamics on the femtosecond timescale in S_1 pyrimidine [90]. The femtosecond pump pulse at 315.3 nm prepared a vibrational

DOI:10.1063/1674-0068/cjcp1811252

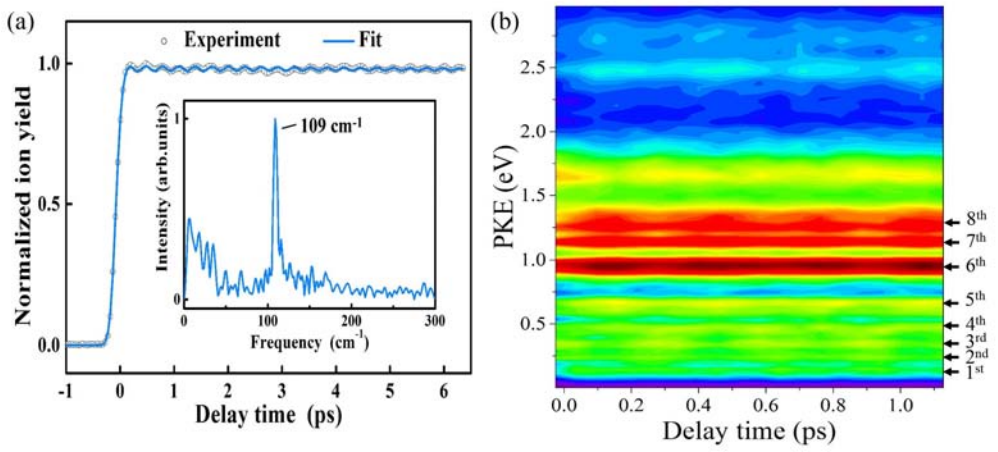

FIG. 5 (a) Time-resolved signals of the parent ion following excitation of *o*-fluorophenol with a 271.3 nm pump pulse and an 802 nm probe pulse. (b) Time-energy map of the PKE distribution. Reprinted with permission from Ref.[82]. Copyright 2017 Nature Publishing Group (http://creativecommons.org/licenses/by/4.0/).

wavepacket merely composed of two known eigenstates of the $6a^1/6b^2$ Fermi doublet in S_1 [84]. Then the femtosecond probe pulse at 398.5 nm interrogated its time evolution into the ion signal and the PKE distribution. The time-resolved intensities of the parent ion exhibited a long-lived decay behavior with a superimposed coherent oscillation. The exponential decay behavior was attributed to the ISC process of the S_1 state. The oscillations arose from coupling between a small number of vibrational states and were a direct signature of restricted IVR. The FFT of the transient exhibited a frequency component at 56 cm^{-1}, resulting in a periodicity of 596 fs, which was in good agreement with the wavenumber separation between one quantum of excitation in 6a and two quanta of excitation in 6b. The observed quantum beat was ascribed to variation in the ionization efficiency as the vibrational wavepacket evolved on the S_1 surface.

As shown in FIG. 6, the time-energy map of the photoelectron intensities is characterized by a clear and regular oscillation. According to the mass-analyzed threshold ionization (MATI) spectra reported by Riese *et al.* [84] and the dynamical behaviors in the present spectra (FIG. 6), we found that the 2nd, 3rd and 4th peaks were from the 3p state and connected to different ion vibrational states. More specifically, ionization of the $6b^2$ state in S_1 was connected to the $6b^{+1}$ and $6b^{+2}$ ion vibrational states, producing the 2nd peak and minor contribution to the 3rd peak, but ionization of the $6a^1$ state was connected to the $6a^{+1}$ and 0^{+0} states, generating the 4th peak and major contribution to the 3rd peak. All of the four peaks oscillated with an identical frequency at 56 cm^{-1}. However, the beats for the 1st and 2nd peaks were out-of-phase with those for the 3rd and 4th peaks, indicating that vibrational population was transferred back and forth between the initially excited states to the dark state. Note that at the instant

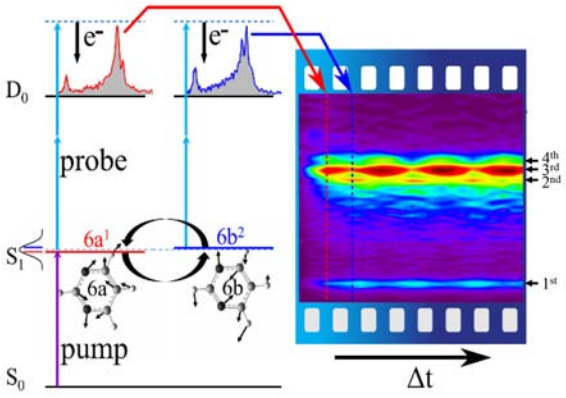

FIG. 6 Schematic depiction of the pump-probe mechanism in pyrimidine. The time-resolved photoelectron spectra are also shown in the right of the figure. Reprinted with permission from Ref.[90]. Copyright 2017 American Institute of Physics.

of excitation, the wavepacket mainly reflected the component character of the $6a^1$ state, with the $6b^2$ characteristic state growing at later time. This suggested that $6a^1$ was a bright state but $6b^2$ was a FC dark state on $S_0 \rightarrow S_1$ excitation. In short, the time-resolved spectra were the direct manifestation of the restricted IVR process that occurred in the $6a^1/6b^2$ Fermi resonance. As discussed above, detection of the ion manifested the periodic variation in the ionization cross section as the quantum beat-modulated decay, and detection of the electron provided the most sensitive means via the variable FC factors between the wavepacket components and the dispersed cation vibrational levels. Both of the two methods provided an unambiguous picture of the vibrational wavepacket dynamics of the $6a^1/6b^2$ Fermi doublet in S_1 pyrimidine.

DOI:10.1063/1674-0068/cjcp1811252

G. 2,4-Difluoroaniline

Understanding the nuclear motions during chemical reactions is one of the fundamental questions in femtochemistry. In a recent study [91], we illustrated the application of femtosecond TR-PEI for watching the reversible and irreversible structural dynamics on a model system 2,4-difluoroaniline (24DFA). According to the calculations using B3LYP/6-311++G(d,p), the geometry optimization of the S_0 state generated a nonplanar structure where the NH_2 part adapted a pyramidal configuration, and S_1 would keep its nonplanar geometry within the vertical FC region. However, the $S_{1,min}$ and $D_{0,min}$ geometries were both planar. The pump-probe transients for the parent ion following 299.8 and 289.0 nm excitation were fitted with the sum of three exponential decays convoluted with a Gaussian cross-correlation function. The picosecond decay corresponded to ISC to the triplet state. And the long-lived component with nanosecond timescale reflected the subsequent slow deactivation process of the triplet state. The femtosecond decay was assigned to an initial geometry rearrangement away from the nonplanar $S_{1,vFC}$ geometry towards the planar minimum.

FIG. 7(a) displayed the time-energy map of the PKE distributions following excitation at 299.8 nm and ionization with 800 nm. These bands exhibited different time evolutions: peaks 2 and 3 could be simulated using a combination of three exponential decays with an exponentially damped oscillation; however, peaks 1, 4, 5, 6, and 7 were simulated with an exponential rise, two exponential decays, and an oscillatory behavior. The observed decay/rise was ascribed to modulation in PKE distribution during the geometry rearrangement process. Both of the fitting data and the FFT for the oscillatory features yielded a major frequency at 89 cm^{-1}, corresponding to a period of 375 fs, which aligned well with the wavenumber separation between the S_1 origin and one quantum of excitation in the out-of-plane vibration X [71]. Obviously, the beats for peaks 2 and 3 exhibited a phase shift of π rad in respect to those for the other peaks, indicating that the vibrational wavepacket oscillated along X. On the basis of the spectral features, peaks 2 and 3 were generated from the nonplanar $S_{1,vFC}$ geometry, and the other peaks were attributed to ionization from the planar $S_{1,min}$ geometry. As the X mode the superstition caused an obvious structural change, leading to periodic variations in the photoionization channel as a function of the molecular geometry. Then the probe pulse directly mapped the wavepacket motion into the superimposed beats.

The time-resolved photoelectron spectra following photoexcitation to S_1 with 1298 cm^{-1} of excess vibrational energy were presented in FIG. 7(b). Interestingly, the quantum beats were absent in the spectra. This suggested that the statistical averaging started to smooth the quantum effects out with the increasing density of vibrational states. By integrating photoelectron signals

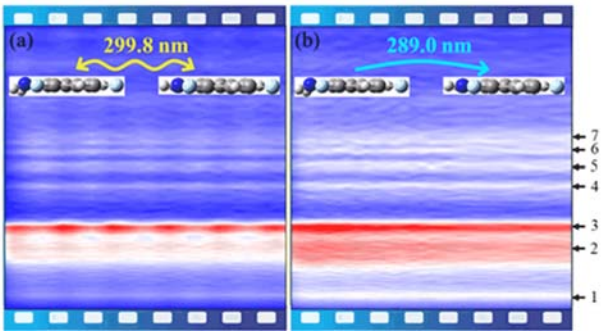

FIG. 7 Photoelectron time-energy map of 24DFA following excitation at (a) 299.8 nm and (b) 289.0 nm and subsequent ionization with 800 nm. Reprinted with permission from Ref.[91]. Copyright 2018 American Chemical Society.

for the first seven peaks, we found an apparently different situation, where peaks numbered 1, 4, 5, 6, and 7 increased but peaks 2 and 3 decreased in intensity as time went by, suggesting the energy transfer from peaks 2 and 3 to the other peaks. The decay/rise phenomenon was assigned to irreversible evolution of the nuclear geometry away from the nonplanar $S_{1,vFC}$ structure towards the energetically more stable planar structure. For the 299.8 nm excitation, a vibrational wavepacket was created in S_1 by the coherent excitation of out-of-plane modes. The involved vibrational modes were very few so that the time-evolving wavepacket moved back and forth along X. The structural changes modulated the photoionization channel, resulting in the out-of-phase beats in the time-resolved photoelectron spectra. For the 289.0 nm excitation, however, the covered density of vibrational states was significantly enhanced, leading to an irreversibly geometry rearrangement in hundreds of femtoseconds.

IV. CONCLUSION

This review has presented a comprehensive discussion of TR-IYS and TR-PEI in application to the studies of vibrational wavepacket dynamics on the excited state surface. The chosen examples include catechol, guaiacol and syringol, CS_2, 2,4-difluorophenol, *o*-fluorophenol, pyrimidine, and 2,4-difluoroaniline. A femtosecond laser pulse with suitable frequency and bandwidth can create a coherent superposition of several vibrational levels, resulting in a vibrational wavepacket. To interrogate this time-evolving wavepacket using TR-IYS, an adequate FC detection window is required and can be afforded by the structural distortion between the S_1 and D_0 geometries. With appropriate choice of probe wavelengths, the signature of vibrational wavepacket dynamics has been observed through the clear beats superimposed on the parent-ion transients. More generally, TR-PEI provides a powerful method for following the time-evolution of the wavepacket because of its

DOI:10.1063/1674-0068/cjcp1811252

sensitivity to both electronic configurations and vibrational dynamics. Photoionization signals from different components of the wavepacket are dispersed and distinguished with respect to kinetic energy and angular distribution. As the time-evolving wavepacket oscillates along the reaction coordinate, the structural changes modulate the photoionization channel, leading to the out-of-phase beats in the time-dependent photoelectron spectra. In addition, parallel theoretical calculations are performed to determine the electronic geometries of the ground, excited, and ionic states and provide supportive interpretation for the experimental data. In short, the present review builds up a detailed picture of how time-dependent photoionization detection (*e.g.*, collection of ion and electron) is employed to follow the evolution of the vibrational wavepacket in photoexcited molecules.

Except for the studies of wavepacket motions, TR-IYS and TR-PEI have been applied to an impressive range of photoinduced reactions. Future applications will benefit from the increasing availability in detector technologies, femtosecond and attosecond laser sources, and nonlinear optical frequency conversion schemes. We expect that the next few years can see a significant improvements in the experimental and theoretical techniques employed in this flourishing area of research. There is a bright future for time-resolved photoionization measurement as a tool to provide deep insight into excited state chemical reactions and enhance our understanding of structure-dynamics-function relationships in complex biological systems.

V. ACKNOWLEDGEMENTS

This work was supported by the National Natural Science Foundation of China (No.21327804, No.21773299, No.91121006, No.21573279, No.11574351, No.11774385, No.11674355, No.21503270, and No.21303255).

[1] T. Gustavsson, R. Improta, and D. Markovitsi, J. Phys. Chem. Lett. **1**, 2025 (2010).
[2] R. Schoenlein, L. Peteanu, R. Mathies, and C. Shank, Science **254**, 412 (1991).
[3] V. G. Stavros and J. R. Verlet, Annu. Rev. Phys. Chem. **67**, 211 (2016).
[4] A. H. Zewail, J. Phys. Chem. A **104**, 5660 (2000).
[5] M. Dantus, M. J. Rosker, and A. H. Zewail, J. Chem. Phys. **87**, 2395 (1987).
[6] L. R. Khundkar and A. H. Zewail, Annu. Rev. Phys. Chem. **41**, 15 (1990).
[7] A. H. Zewail, Angew. Chem. Int. Ed. **39**, 2586 (2000).
[8] C. Rischel, A. Rousse, I. Uschmann, P. A. Albouy, J. P. Geindre, P. Audebert, J. C. Gauthier, E. Fröster, J. L. Martin, and A. Antonetti, Nature **390**, 490 (1997).
[9] A. Chin, R. Schoenlein, T. Glover, P. Balling, W. Leemans, and C. Shank, Phys. Rev. Lett. **83**, 336 (1999).
[10] J. R. Dwyer, C. T. Hebeisen, R. Ernstorfer, M. Harb, V. B. Deyirmenjian, R. E. Jordan, and R. D. Miller, Philos. Trans. R. Soc. London, Ser. A **364**, 741 (2006).
[11] M. Eichberger, H. Schäfer, M. Krumova, M. Beyer, J. Demsar, H. Berger, G. Moriena, G. Sciaini, and R. D. Miller, Nature **468**, 799 (2010).
[12] S. Pedersen, J. Herek, and A. Zewail, Science **266**, 1359 (1994).
[13] H. Goto, H. Katsuki, H. Ibrahim, H. Chiba, and K. Ohmori, Nat. Phys. **7**, 383 (2011).
[14] M. Corrales, J. González-Vázquez, G. Balerdi, I. Solá, R. De Nalda, and L. Bañares, Nat. Chem. **6**, 785 (2014).
[15] Y. Liu, G. Knopp, C. Qin, and T. Gerber, Chem. Phys. **446**, 142 (2015).
[16] A. Lietard, G. Piani, L. Poisson, B. Soep, J. M. Mestdagh, S. Aloïse, A. Perrier, D. Jacquemin, and M. Takeshita, Phys. Chem. Chem. Phys. **16**, 22262 (2014).
[17] J. Davies, R. Continetti, D. Chandler, and C. Hayden, Phys. Rev. Lett. **84**, 5983 (2000).
[18] Y. Z. Liu, J. Y. Long, L. H. Xu, X. Y. Zhang, and B. Zhang, Chin. Phy. Lett. **34**, 033301 (2017).
[19] D. Horke, H. Watts, A. Smith, E. Jager, E. Springate, O. Alexander, C. Cacho, R. Chapman, and R. Minns, Phys. Rev. Lett. **117**, 163002 (2016).
[20] S. Lochbrunner, T. Schultz, M. Schmitt, J. Shaffer, M. Zgierski, and A. Stolow, J. Chem. Phys. **114**, 2519 (2001).
[21] G. M. Roberts, C. A. Williams, J. D. Young, S. Ullrich, M. J. Paterson, and V. G. Stavros, J. Am. Chem. Soc. **134**, 12578 (2012).
[22] G. A. King, T. A. Oliver, and M. N. Ashfold, J. Chem. Phys. **132**, 214307 (2010).
[23] Y. I. Suzuki, T. Fuji, T. Horio, and T. Suzuki, J. Chem. Phys. **132**, 174302 (2010).
[24] Y. Liu, G. Knopp, and T. Gerber, Phys. Rev. A **92**, 042501 (2015).
[25] Y. Liu, T. Gerber, C. Qin, F. Jin, and G. Knopp, J. Chem. Phys. **144**, 084201 (2016).
[26] F. Ling, S. Li, J. Wei, K. Liu, Y. Wang, and B. Zhang, J. Chem. Phys. **148**, 144311 (2018).
[27] J. A. Davies, A. M. Green, and K. L. Reid, Phys. Chem. Chem. Phys. **12**, 9872 (2010).
[28] Y. Yamada, N. Mikami, and T. Ebata, J. Chem. Phys. **121**, 11530 (2004).
[29] S. Li, F. Ling, Y. Wang, J. Long, X. Deng, B. Jin, and B. Zhang, Phys. Rev. A **96**, 033419 (2017).
[30] A. Assion, M. Geisler, J. Helbing, V. Seyfried, and T. Baumert, Phys. Rev. A **54**, R4605 (1996).
[31] D. M. Neumark, Annu. Rev. Phys. Chem. **52**, 255 (2001).
[32] K. L. Reid, Annu. Rev. Phys. Chem. **54**, 397 (2003).
[33] T. Suzuki, Annu. Rev. Phys. Chem. **57**, 555 (2006).
[34] G. Wu, P. Hockett, and A. Stolow, Phys. Chem. Chem. Phys. **13**, 18447 (2011).
[35] R. Carley, E. Heesel, and H. Fielding, Chem. Soc. Rev. **34**, 949 (2005).
[36] M. N. R. Ashfold, N. H. Nahler, A. J. Orr-Ewing, O. P. J. Vieuxmaire, R. L. Toomes, T. N. Kitsopoulos, I. A. Garcia, D. A. Chestakov, S. M. Wu, and D. H. Parker, Phys. Chem. Chem. Phys. **8**, 26 (2006).
[37] H. H. Fielding and G. A. Worth, Chem. Soc. Rev. **47**, 309 (2018).
[38] A. Stolow, A. E. Bragg, and D. M. Neumark, Chem.

DOI:10.1063/1674-0068/cjcp1811252

Rev. **104**, 1719 (2004).
[39] W. Heisenberg, in *Original Scientific Papers Wissenschaftliche Originalarbeiten*, Berlin: Springer, 478 (1985).
[40] P. M. Felker and A. H. Zewail, Phys. Rev. Lett. **53**, 501 (1984).
[41] W. Wiley and I. H. McLaren, Rev. Sci. Instrum. **26**, 1150 (1955).
[42] D. W. Chandler and P. L. Houston, J. Chem. Phys. **87**, 1445 (1987).
[43] A. T. Eppink and D. H. Parker, Rev. Sci. Instrum. **68**, 3477 (1997).
[44] C. Vallance, Philos. Trans. R. Soc. Lond. A **362**, 2591 (2004).
[45] V. Dribinski, A. Ossadtchi, V. A. Mandelshtam, and H. Reisler, Rev. Sci. Instrum. **73**, 2634 (2002).
[46] G. A. Garcia, L. Nahon, and I. Powis, Rev. Sci. Instrum. **75**, 4989 (2004).
[47] G. Roberts, J. Nixon, J. Lecointre, E. Wrede, and J. Verlet, Rev. Sci. Instrum. **80**, 053104 (2009).
[48] C. Z. Bisgaard, O. J. Clarkin, G. Wu, A. M. Lee, O. Geßner, C. C. Hayden, and A. Stolow, Science **323**, 1464 (2009).
[49] R. R Lucchese and A. Stolow, J. Phys. B **45**, 190201 (2012).
[50] A. L. Sobolewski and W. Domcke, Chem. Phys. Chem. **8**, 756 (2007).
[51] A. Huijser, A. Pezzella, and V. Sundström, Phys. Chem. Chem. Phys. **13**, 9119 (2011).
[52] A. S. Chatterley, J. D. Young, D. Townsend, J. M. Żurek, M. J. Paterson, G. M. Roberts, and V. G. Stavros, Phys. Chem. Chem. Phys. **15**, 6879 (2013).
[53] G. A. King, T. A. Oliver, R. N. Dixon, and M. N. Ashfold, Phys. Chem. Chem. Phys. **14**, 3338 (2012).
[54] R. A. Livingstone, J. O. Thompson, M. Iljina, R. J. Donaldson, B. J. Sussman, M. J. Paterson, and D. Townsend, J. Chem. Phys. **137**, 184304 (2012).
[55] J. Young, M. Staniforth, M. J. Paterson, and V. Stavros, Phys. Rev. Lett. **114**, 233001 (2015).
[56] M. Gerhards, S. Schumm, C. Unterberg, and K. Kleinermanns, Chem. Phys. Lett. **294**, 65 (1998).
[57] J. D. Young, M. Staniforth, J. C. Dean, G. M. Roberts, F. Mazzoni, T. N. Karsili, M. N. Ashfold, T. S. Zwier, and V. G. Stavros, J. Phys. Chem. Lett. **5**, 2138 (2014).
[58] J. C. Dean, P. Navotnaya, A. P. Parobek, R. M. Clayton, and T. S. Zwier, J. Chem. Phys. **139**, 10B609_1 (2013).
[59] R. Wu and B. Brutschy, Chem. Phys. Lett. **390**, 272 (2004).
[60] A. Longarte, C. Redondo, J. A. Fernández, and F. Castaño, J. Chem. Phys. **122**, 164304 (2005).
[61] T. Fuji, Y. I. Suzuki, T. Horio, and T. Suzuki, Chem. Asian J. **6**, 3028 (2011).
[62] R. Hemley, D. Leopold, J. Roebber, and V. Vaida, J. Chem. Phys. **79**, 5219 (1983).
[63] A. Douglas and I. Zanon, Can. J. Phys. **42**, 627 (1964).
[64] A. Beatty, R. Shiell, D. Chang, and J. Hepburn, J. Chem. Phys. **110**, 8476 (1999).
[65] P. Farmanara, V. Stert, and W. Radloff, J. Chem. Phys. **111**, 5338 (1999).
[66] D. Townsend, H. Satzger, T. Ejdrup, A. M. Lee, H. Stapelfeldt, and A. Stolow, J. Chem. Phys. **125**, 234302 (2006).
[67] P. Hockett, C. Z. Bisgaard, O. J. Clarkin, and A. Stolow, Nat. Phys. **7**, 612 (2011).
[68] R. Spesyvtsev, T. Horio, Y. I. Suzuki, and T. Suzuki, J. Chem. Phys. **142**, 074308 (2015).
[69] S. G. He and D. J. Clouthier, J. Chem. Phys. **124**, 084312 (2006).
[70] F. Ling, S. Li, X. Song, Y. Tang, Y. Wang, and B. Zhang, Phys. Rev. A **95**, 043421 (2017).
[71] W. C. Huang, P. S. Huang, C. H. Hu, and W. B. Tzeng, Spectrochim. Acta, Part A **93**, 176 (2012).
[72] C. Y. Tsai and W. B. Tzeng, J. Photochem. Photobiol. A **270**, 53 (2013).
[73] V. Shivatare and W. B. Tzeng, Bull. Korean. Chem. Soc. **35**, 815 (2014).
[74] A. Oikawa, H. Abe, N. Mikami, and M. Ito, Chem. Phys. Lett. **116**, 50 (1985).
[75] Q. Zheng, C. Qin, J. Long, B. Tang, S. Zhang, and B. Zhang, Sci. China **53**, 1040 (2010).
[76] L. Yuan, C. Li, J. L. Lin, S. C. Yang, and W. B. Tzeng, Chem. Phys. **323**, 429 (2006).
[77] N. Tsuji, S. I. Ishiuchi, M. Sakai, M. Fujii, T. Ebata, C. Jouvet, and C. Dedonder-Lardeux, Phys. Chem. Chem. Phys. **8**, 114 (2006).
[78] K. Remmers, W. L. Meerts, A. Zehnacker-Rentien, K. Le Barbu, and F. Lahmani, J. Chem. Phys. **112**, 6237 (2000).
[79] A. Kovács, V. Izvekov, G. Keresztury, C. J. Nielsen, and P. Klæboe, Chem. Phys. **335**, 205 (2007).
[80] T. Omi, H. Shitomi, N. Sekiya, K. Takazawa, and M. Fujii, Chem. Phys. Lett. **252**, 287 (1996).
[81] E. Fujimaki, A. Fujii, T. Ebata, and N. Mikami, J. Chem. Phys. **110**, 4238 (1999).
[82] F. Ling, S. Li, X. Song, Y. Wang, J. Long, and B. Zhang, Sci. Rep. **7**, 15362 (2017).
[83] J. Philis, J. Mol. Spectrosc. **232**, 26 (2005).
[84] M. Riese and J. Grotemeyer, Anal. Bioanal. Chem. **386**, 59 (2006).
[85] A. Bolovinos, P. Tsekeris, J. Philis, E. Pantos, and G. Andritsopoulos, J. Mol. Spectrosc. **103**, 240 (1984).
[86] S. Ghanta, Mol. Phys. **114**, 2958 (2016).
[87] G. Fischer, Z. L. Cai, J. R. Reimers, and P. Wormell, J. Phys. Chem. A **107**, 3093 (2003).
[88] J. H. Kim, J. H. Lee, H. Hwang, H. L. Kim, and C. H. Kwon, Phys. Chem. Chem. Phys. **16**, 1590 (2014).
[89] W. Wolff, H. Luna, L. Sigaud, A. C. Tavares, and E. C. Montenegro, J. Phys. Chem. A **140**, 064309 (2014).
[90] S. Li, J. Long, F. Ling, Y. Wang, X. Song, S. Zhang, and B. Zhang, J. Chem. Phys. **147**, 044309 (2017).
[91] F. Ling, Y. Wang, S. Li, J. Wei, Y. Tang, and B. Zhang, J. Phys. Chem. Lett. **9**, 5468 (2018).

DOI:10.1063/1674-0068/cjcp1811252